energies

MDPI

Article

Dynamic Boost Based DMPPT Emulator

Marco Balato *,†, Annalisa Liccardo † and Carlo Petrarca †

Department of Electrical Engineering and Information Technologies, University of Naples "Federico II", Via Claudio 21 – 80125 Napoli, Italy, annalisa.liccardo@unina.it (A.L.); carlo.petrarca@unina.it (C.P.)

* Correspondence: marco.balato@unina.it

† These authors contributed equally to this work.

Received: 8 May 2020; Accepted: 4 June 2020; Published: 6 June 2020

Abstract: The Distributed Maximum Power Point Tracking (DMPPT) approach is a promising solution to improve the energetic performance of mismatched PhotoVoltaic (PV) systems. However, there are still several factors that can reduce DMPPT energy efficiency, including atmospheric conditions, the efficiency of the power stage, constraints imposed by the topology, the finite rating of silicon devices, and the nonoptimal value of string voltage. In order to fully explore the advantages offered by the above solution, the implementation of a Boost based DMPPT emulator is of primary concern, especially if it behaves as a controlled voltage or current source. The repeatability of experimental tests, the tighter control of climatic conditions, the closing of the gap between the physical dimensions of a PV array and the space available in a university lab, the simplicity with which new algorithms can be tested, and the low maintenance costs are just some of the benefits offered by an emulator. This paper describes the realization and use of a Boost based Distributed Maximum Power Point Tracking (DMPPT) emulator and shows its high flexibility and potential. The device is able to emulate the output current vs. voltage (*I-V*) characteristics of many commercial PhotoVoltaic (PV) modules with a dedicated Boost DC/DC converter. The flexibility is guaranteed by the ability to reproduce both $I = f(V)$ and $V = g(I)$ characteristics at different values of not only the irradiance levels but also the maximum allowed voltage across the switching devices. The system design is based on a commercial power supply controlled by a low-cost Arduino board by Arduino (Strambino, Torino, Italy). Data acquisition is performed through a low-cost current and voltage sensor by using a multichannel board by National Instruments. Experimental results confirm the capability of the proposed device to accurately emulate the output *I-V* characteristic of Boost based DMPPT systems obtained by varying the atmospheric conditions, the rating of silicon devices, and the electrical topology.

Keywords: distributed maximum power point tracking; mismatching; PV emulator

1. Introduction

Climate change and environmental degradation are issues of concern in the present world and represent the main challenges that we will face in the near future in order to prevent adverse socioeconomic consequences. A crucial aspect of Green New Deal action will be to decarbonize the production of electricity using renewable energy sources. To reinforce the distributed green energy generation, which represents another important challenge, photovoltaic (PV) systems are among the most promising renewable sources. In the last 20 years, the main objective of the scientific community has been to fully understand the factors that limit the energetic performance of PV systems [1–7] and propose possible solutions [8–38]. What emerges is that commonly used grid-connected PV installations, made of strings of PV modules connected in parallel and feeding a central inverter, are ineffective when mismatching conditions occur (due to clouds, shadows, dirt, etc.).

In order to overcome the above limitations, several solutions have been presented in the literature, such as high-performance Maximum Power Point Tracking (MPPT) techniques [8–16], reconfiguration architectures [17–26], distributed MPPT techniques [27–38], and so on. The Distributed Maximum Power Point Tracking (DMPPT) approach is by far the most hopeful solution to improve the energetic performance of mismatched PV systems. However, there are still several factors that can reduce DMPPT energy efficiency, including atmospheric conditions, the efficiency of the power stage, constraints imposed by the topology, the finite rating of silicon devices, and the nonoptimal value of string voltage [36–40]. The fact that many of these factors are not under our control represents an objective difficulty in conducting experimental test activities when real DMPPT PV systems are considered. The need for DMPPT emulators, as described in greater detail in Section 2, is a natural consequence of the above drawbacks.

The present paper presents a DMPPT emulator of which the main advantage is the possibility to reproduce both $I = f(V)$ and $V = g(I)$ characteristics of commercial PV modules at different values of not only the irradiance levels (as happens for common PV emulators [39–42]) but also maximum allowed voltage across the switching devices. The high flexibility offered by the proposed device makes it suitable for testing traditional or innovative solutions such as the DMPPT and the reconfiguration approach, or a combination of both [38]. The designed emulator consists of a commercial power supply controlled by a low-cost Arduino board. The control strategy is based on a set of equations defining the mathematical model of a DMPPT device.

The paper is organized as follows: the necessity for a DMPPT emulator is presented in Section 2; the mathematical model of a single Boost based DMPPT unit is described in detail in Section 3; Section 4 is dedicated to the design and description of the proposed Boost based DMPPT emulator; experiments and tests are presented in Sections 5; and finally, Section 6 presents the conclusions.

2. Necessity for DMPPT Emulator

The DMPPT approach represents the most promising solution to counteract the negative effects of mismatching phenomena, which have deep repercussions on the energetic efficiency and reliability of the entire PV system. Two DMPPT approaches can be used: DC/AC (microinverter) based [27–29], and DC/DC converter based [30–32]. Hereafter, without any loss of generality, we will refer to the second solution. A typical schematic representation of a grid-connected PV system with DMPPT is shown in Figure 1. The system, composed of a PV module with a dedicated DC/DC converter implementing the MPPT function, is indicated as PVU (PV unit).

As shown in [32–37], the DC/DC converter topologies suitable for DMPPT applications are Buck, Boost, and Buck–Boost topologies. Buck–Boost is characterized by lower efficiency and higher cost as a result of enhanced component stresses. In [32–36], it is shown that maximum energy productivity of the Buck–Boost converter is guaranteed only in cases in which the mismatch conditions are quite heavy. The Buck converter works optimally especially in PV systems characterized by a light mismatching scenario or when, for example, shade or mismatch occurs on only a few PV modules. In this case, the Buck DC/DC converter can be installed only on those PV modules experiencing shade [32–36]. Moreover, due to the step-down conversion ratio, a consistent number of Buck converters is necessary in order to obtain string voltage compatible with the input inverter voltage, with a resulting increase in operating cost. Finally, the Boost converter, thanks to the lower voltage stress, which reduces the undesired action of voltage limiting in mismatching conditions and allows election of devices with lower channel resistance, can ensure overall DMPPT effectiveness in a wider range of possible mismatching conditions [36].

On the basis of the aforementioned considerations, if a reasonable, fair comparison among topologies is carried out, by taking into account power stage efficiency, cost, voltage, and current stress of components and therefore their reliability, it can be concluded that a suitable compromise solution for series-connected DC/DC converters installed on all PV modules of the string is generally the Boost converter. For this reason, in the following, we refer to Boost based DMPPT. Nevertheless, there are many factors that restrict Boost based DMPPT energetic performance, including atmospheric conditions, the efficiency of the power stage, constraints imposed by the topology, and

the finite rating of the silicon devices [32–38]. The above factors together with the nonoptimal value of the string voltage (V_{string}) make the efficiency $\eta_{DMPPT} < 1$.

In order to clarify the above assumptions, it can be useful to compare two systems with the same topology, formed by series connection of two PV panels: in the first system (Figure 2a), DMPPT architecture is implemented; in the second system, the Central Maximum Power Point Tracking (CMPPT) function is adopted (Figure 2b). The electrical characteristics of commercial PV modules (Sunmodule SW225 by SolarWorld industries (Bonn, Germany) [43]) in standard test conditions (STC; $T_{STC} = 25$ °C, $S_{STC} = 1000$ W/m^2) are reported in Table 1.

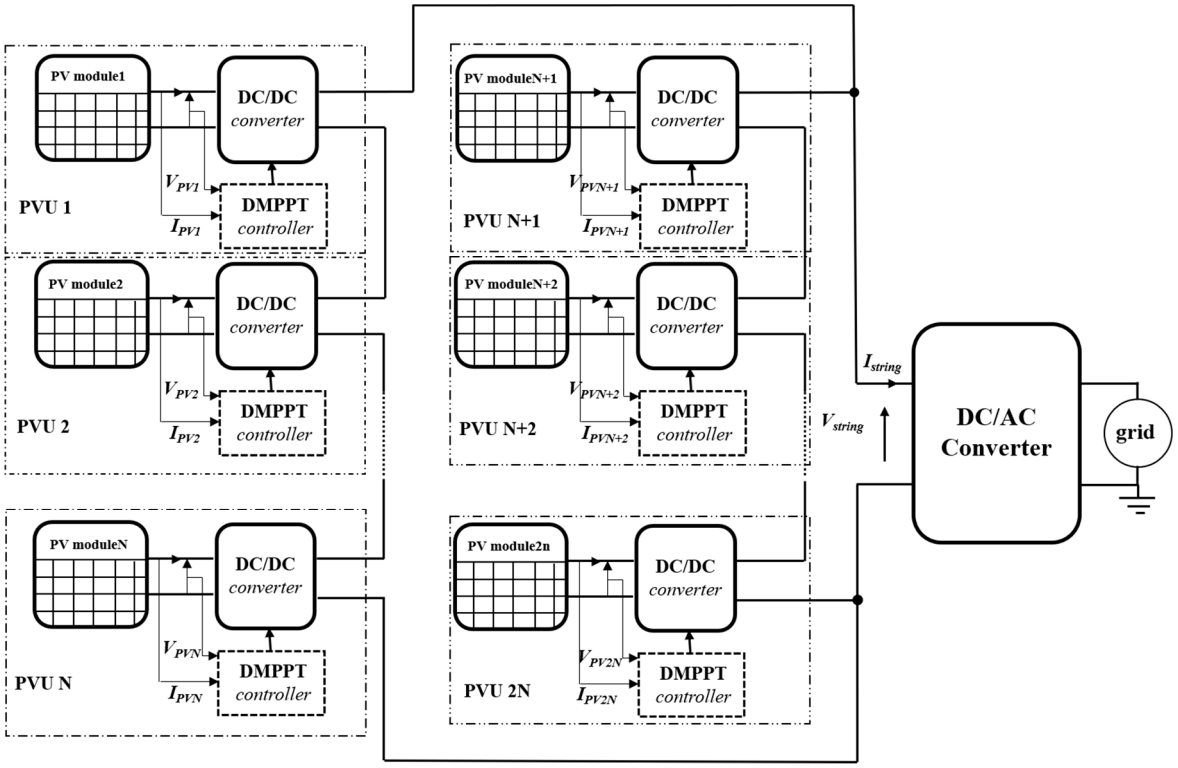

Figure 1. Grid-connected PhotoVoltaic (PV) system with Distributed Maximum Power Point Tracking (DMPPT).

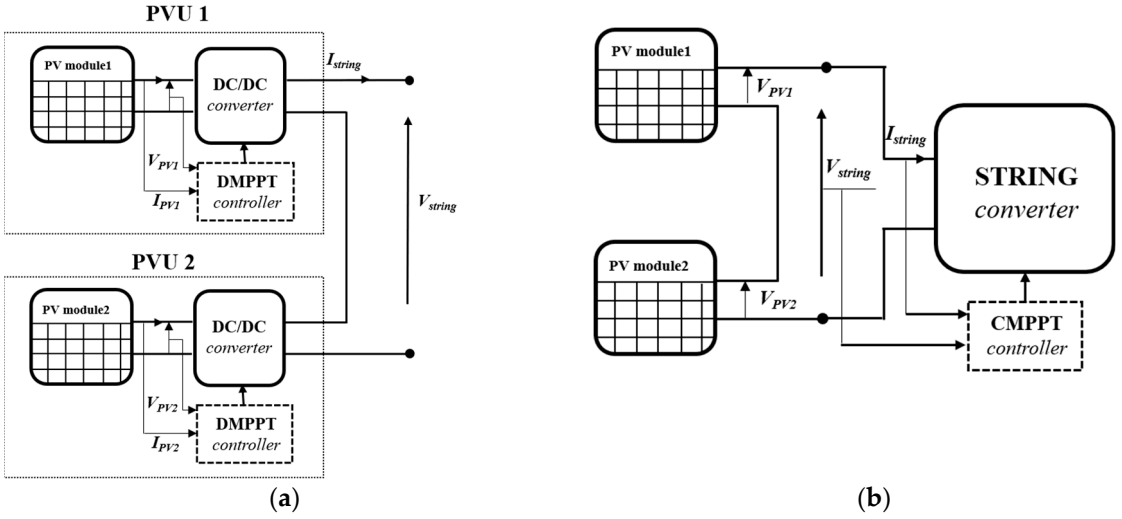

Figure 2. Systems under test: (**a**) DMPPT PV System; (**b**) Central Maximum Power Point Tracking (CMPPT) PV system.

Different from DMPPT, the central approach performs its MPPT function on the entire PV plant rather than on each PV module.

Table 1. SolarWorld SW 225 PV module electrical characteristics in standard test conditions (STC).

($S_{STC} = 1000$ W/m^2, $T_{STC} = 25$ °C).	
STC open circuit voltage	$V_{OC_{STC}} = 36.7$ V
STC short circuit current	$I_{SC_{STC}} = 8.13$ A
STC maximum power point voltage	$V_{MPP_{STC}} = 29.7$ V
STC maximum power point current	$I_{MPP_{STC}} = 7.59$ A
Voltage temperature coefficient	$\alpha_V = -0.34$ %/K
Current temperature coefficient	$\alpha_I = 0.034$ %/K
Nominal Operating Cell Temperature	$NOCT = 46$ °C

In order to show and compare the energy performance of both systems, we can calculate their performance ratio (*PR*):

$$PR = \frac{P_{MAX}}{P_{AV}} = \frac{P_{MAX}}{P_{MPP_1} + P_{MPP_2}} \quad (1)$$

in which $\boldsymbol{P_{MAX}}$ represents the maximum power that can be extracted from the PV system in the considered atmospheric conditions, and $\boldsymbol{P_{AV}}$ is the available maximum power obtained by the sum of maximum power ($\boldsymbol{P_{MPP_1}}, \boldsymbol{P_{MPP_2}}$) that each shaded PV module is able to provide.

The performance ratio is a function of the mismatching degree (MD) and the maximum allowed voltage V_{dsmax} provided by silicon devices, where MD is defined as:

$$\boldsymbol{MD} = \left(\mathbf{1} - \frac{\boldsymbol{S_1}}{\boldsymbol{S_1}}\right) \quad (2)$$

where $\boldsymbol{S_1}$, $\boldsymbol{S_1}$ are the irradiance values of modules 1 and 2.

In Figure 3, the PRs are plotted as a function of MD and voltage V_{dsmax}.

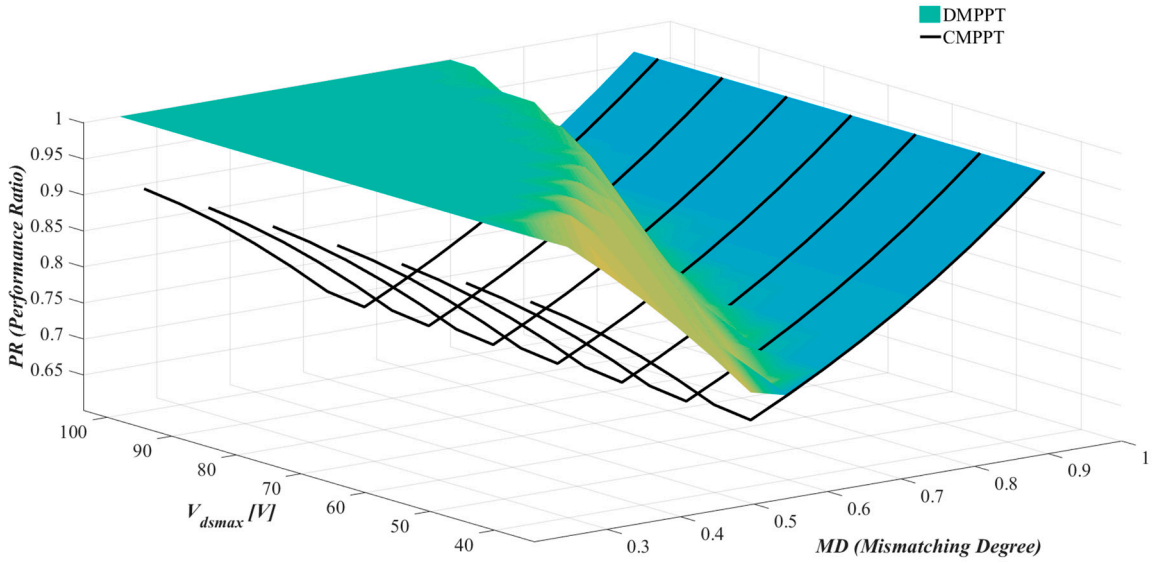

Figure 3. Performance ratio as a function of mismatching degree of the value assumed by V_{dsmax}.

Figure 3 shows that for low values of *MD*, the energetic performance of the DMPPT approach is far superior than that obtained by CMPPT ($PR_{DMPPT} > PR_{CMPPT}$). The same consideration cannot be extended for high values of *MD*, in that the difference between the two approaches does not promote employing one DC/DC converter for each PV module. Moreover, by looking at Figure 3, it is clear

that the value of MD where $PR_{DMPPT} > PR_{CMPPT}$ strongly depends on the maximum allowed voltage V_{dsmax} provided by the silicon devices.

Moreover, it should also be considered that the value assumed by the string voltage seriously undermines the power extracted from the entire DMPPT PV system, if it does not belong to the best operating voltage (BOV) interval, as shown in Figure 4, which, as an example, shows the Performance ratio vs. Voltage characteristics obtained when $MD = 0.4$ and $V_{dsmax} = 60$ V.

Recent studies have shown the positive impact of the combined action of the distributed approach and dynamic reconfiguration from a broader perspective compared with approaches closely related to the extracted power, by taking into account not only the efficiency but also the reliability of the entire PV system [38]. In order to fully explore the advantages offered by the above solution, the implementation of a Boost based DMPPT emulator is of primary concern, especially if it behaves as a controlled voltage or current source.

The repeatability of experimental tests, the tighter control of climatic conditions, the closing of the gap between the physical dimensions of a PV array and the space available in a university lab, the simplicity with which new algorithms can be tested, and the low maintenance costs are just some of the benefits offered by an emulator. Moreover, it is also evident that, in order to deeply understand the real potential of the DMPPT approach, a huge number of Boost converters, characterized by different V_{dsmax} values, are necessary. In fact, as shown before, silicon devices have a great influence on the achievement of high energy efficiency due to their finite voltage ratings. The enormous effort required in terms of both time and cost could be partly lessened by adopting a Boost based DMPPT emulator that foresees the possibility to swap the value of V_{dsmax}.

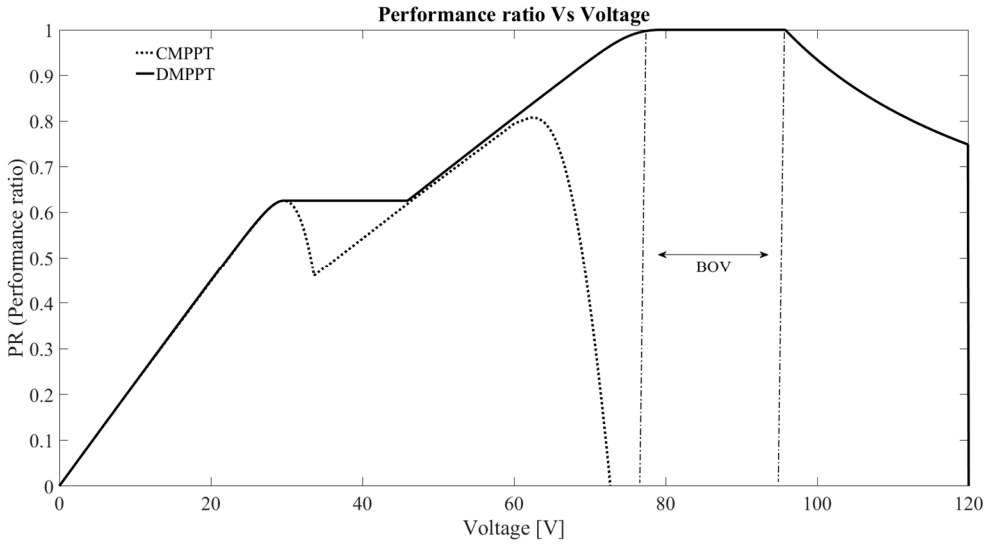

Figure 4. Performance ratio vs. voltage of series connection of two Boost based photovoltaic units (PVUs) ($V_{dsmax} = 60$ V, $MD = 0.4$).

3. Mathematical Model of Boost Based PVU

A Boost based photovoltaic unit is shown in Figure 5. In the above figure, I_{ph} is the photo-induced current; diode D_1 takes into account the effects at the silicon p–n junction of a PV cell; losses are considered by inserting series resistance R_S and shunt resistance R_{sh}; I_{PV} (V_{PV}) and I_{PVU} (V_{PVU}) are currents (voltages) at the input and output ports of the converter, respectively. The typical output static Current vs. Voltage (*I-V*) characteristics of a PV module (dashed line) and a controlled PV module (bold line) are represented, at constant irradiance (S) and temperature (T) values, in Figure 6. Losses occurring in the power stage of the Boost converter (switching, conduction, and iron losses) and the settling time of the step response of a closed or open loop PVU are neglected. In the following, in order to take the dynamic behavior of the considered system into account, a time delay will be

introduced. The *I-V* curve is composed of three operating regions, OR1, OR2, and OR3, described in the following.

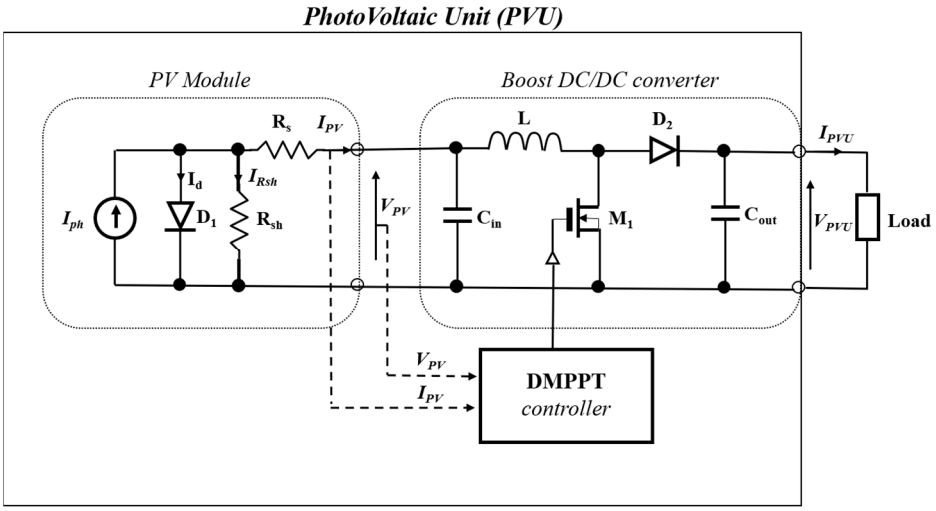

Figure 5. Circuit model of Boost based PVU.

Operating region 1: OR1 is defined for $0 \le V_{PVU} \le V_{MPP}$, where V_{MPP} is the MPP voltage that can be provided by the adopted PV module in the considered atmospheric conditions:

$$V_{MPP} = V_{MPP_{STC}}\left[1 + \frac{\alpha_V}{100}(T - T_{STC})\right] \quad (3)$$

where α_V is the temperature coefficient of the voltage [44].

In such a region, the two characteristics of the PV module and the controlled PV module are coincidental. In fact, for $0 \le V_{PVU} < V_{MPP}$, the MPPT controller forces the Boost DC/DC converter to work with a duty cycle equal to one. In this condition it gives:

$$I_{PVU} = I_{PV} = I_{ph} - I_d - I_{Rsh} \quad (4)$$

where I_{ph} is the photo-induced current, which, in accordance with Equation (5), is linearly dependent on the irradiance level (S) and the PV module temperature (T), I_d is the current in diode D_1 (Equation (6)), and I_{Rsh} is the shunt-resistor current (Equation (7)):

$$I_{ph} = I_{SC,STC}\frac{S}{S_{STC}}\left(1 + \frac{\alpha_I}{100}(T - T_{STC})\right) \quad (5)$$

$$I_d = I_{sat}\left(e^{\frac{V_{PV} + R_S I_{PV}}{V_T}} - 1\right) \quad (6)$$

$$I_{Rsh} = \frac{V_{PV} + R_S \cdot I_{PV}}{R_{sh}} \quad (7)$$

where V_T is the thermal voltage and I_{sat} is the diode reverse bias saturation current (Equation (8)):

$$I_{sat} = CT^3 e^{\left(-\frac{E_{gap}}{kT}\right)} \quad (8)$$

where $k = 1.38$ J/K is the Boltzmann constant, E_{gap} is the band gap of the semiconductor material (in the following it is assumed $E_{gap} = 1.124$ eV), and C is the temperature coefficient [44].

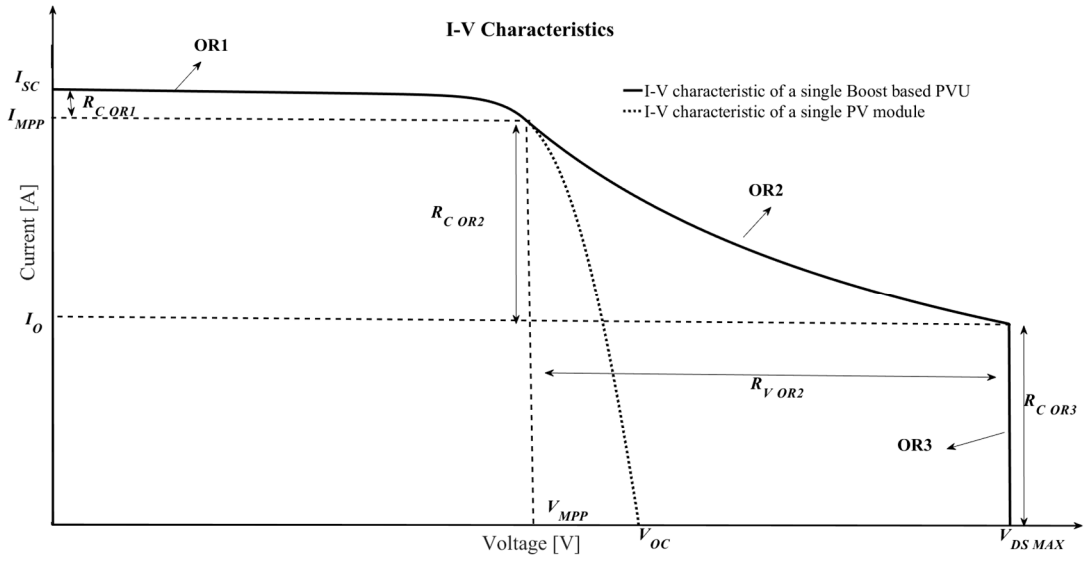

Figure 6. PV module I-V characteristic and Boost based PVU *I-V* characteristics.

Operating region 2: OR2, defined for $V_{MPP} < V_{PVU} \leq V_{dsmax}$, is described by a hyperbole of Equation (9), where V_{dsmax} is the maximum allowed voltage provided by the mosfet M_1 (Figure 5).

$$V_{PVU} \cdot I_{PVU} = P_{MPP} \tag{9}$$

As shown in Figure 6, the current range ($R_{C\,OR2}$) associated with OR2 is as follows:

$$R_{C\,OR2} = [I_O, I_{MPP}] \tag{10}$$

where I_{MPP} is the MPP current, the value of which is obtained by using Equation (4), setting in Equations (6) and (7) the value of V_{PV} is equal to V_{MPP}, I_0 is the value of I_{PVU} when $V_{PVU} = V_{dsmax}$ (Equation (11)).

$$I_O = \frac{P_{MPP}}{V_{dsmax}} \tag{11}$$

Operating region 3: OR3 is defined by a vertical drop occurring at $V_{PVU} = V_{dsmax}$, due to the action of the output overvoltage protection circuitry. The current range ($R_{C\,OR3}$) referring to OR3 is:

$$R_{C\,OR3} = [0, I_0] \tag{12}$$

The *I-V* output characteristics of a single PVU are strictly dependent on the irradiance and temperature levels (Equation (13)). As shown in Table 1, the acronym *NOCT* means Nominal Operating Cell Temperature. Typical curves are shown in Figure 7.

$$T = T_{ambient} + \frac{NOCT - 20}{800} S \tag{13}$$

It is worth noting that in real environmental conditions, the temperature usually changes quite slowly with respect to variation of the irradiance level occurring during the day. Based on this, all subsequent results were obtained by considering a constant value of the PV module temperature of $T = 57.5\ ^\circ\mathrm{C}$ ($T_{ambient} = 25\ ^\circ\mathrm{C}$).

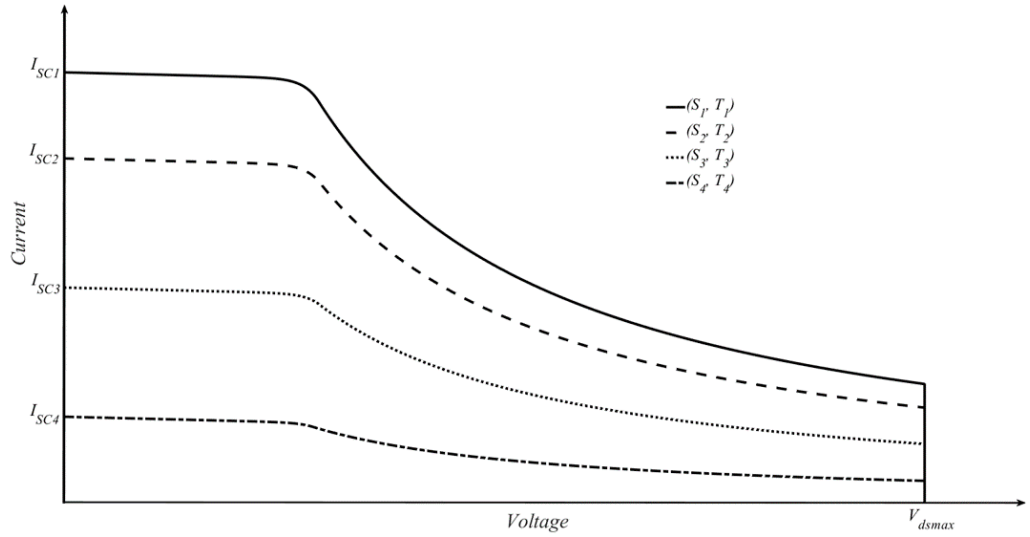

Figure 7. *I-V* characteristics of Boost-based PVU.

4. Design and Implementation of Boost Based PVU Emulator

A block diagram of the proposed Boost based PVU emulator is shown in Figure 8. The emulator is characterized by its simplicity of implementation and high flexibility. In order to be easily reconfigured, it consists of a current (voltage) controlled power supply, in which the output current $I_{PVU}(t)$ (voltage $V_{PVU}(t)$) is regulated by means of a proper controller. In other words, the system acts either as a controlled voltage source, if there is the need for a series connection, or as a controlled current source, if there is the need for a parallel connection.

The input signals to the controlling unit are: $V_{PVU}(t)$ (PVU output voltage), $I_{PVU}(t)$ (PVU output current), V_{dsmax} (voltage signal, which is proportional to the maximum allowed voltage supported by the converter's mosfet M1), $V_S(t)$ (time-varying voltage signal, which is proportional to desired irradiance level S; Equation (14)), and $V_{td}(t)$ (voltage signal, which is proportional to the PV system settling time t_d; Equation (15)):

$$V_S(t) = \alpha_S \, S(t) \tag{14}$$

$$V_{td}(t) = \alpha_{td} \, t_d \tag{15}$$

with $\boldsymbol{\alpha_S = 1\ [V\ m^2/W]}$ and $\boldsymbol{\alpha_{td} = 1\ [V/s]}$. Corresponding with standard irradiance $\boldsymbol{S_{STC}}$, $\boldsymbol{V_S(t)}$ assumes the value $\boldsymbol{V_{SSTC}}$; corresponding with the maximum settling time $\boldsymbol{t_{dMAX}}$, $\boldsymbol{V_{td}(t)}$ assumes the value $\boldsymbol{V_{tdMAX}}$. The calculation of $\boldsymbol{t_{dMAX}}$ is reported in Appendix A. The output signal $\boldsymbol{S_{ref}(t)}$ attained by the conditioning process is calculated according to the diagram shown in Figure 9. It depends on the operating region of the PV unit and is a proper function of the input signals ($\boldsymbol{V_{PVU}(t)}$, $\boldsymbol{I_{PVU}(t)}$, $\boldsymbol{V_S(t)}$, $\boldsymbol{V_{td}(t)}$ and $\boldsymbol{V_{dsmax}}$). It includes a digital signal (CTR), which is settled in a high (low) state if a voltage (current) controlled source is needed. A proper digital analog converter (DAC) is used to obtain CTR.

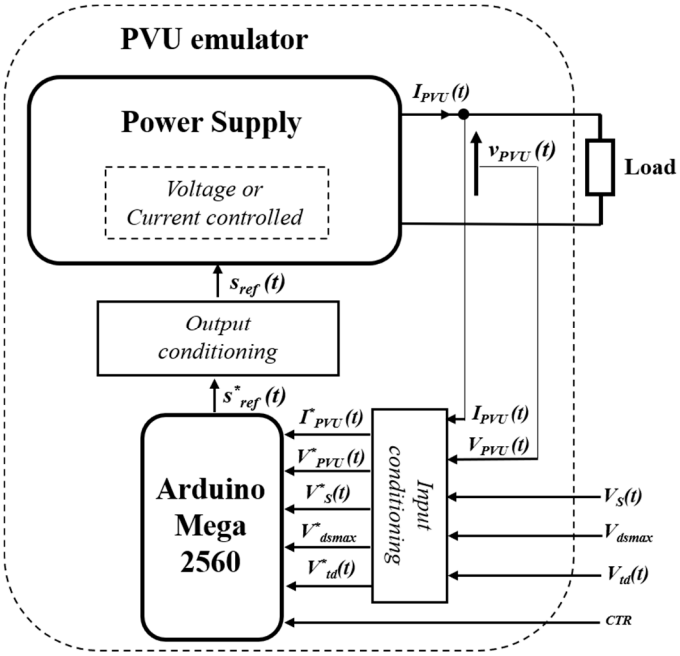

Figure 8. Block diagram of proposed PVU emulator.

As highlighted in Figure 8, the core of the proposed PVU emulator is represented by an Arduino Mega 2560 microcontroller. Such a device can be programmed by means of Arduino IDE software by Arduino (Strambino, Torino, Italy), which is freely available online [45]. As one might expect, the analog input signals of the microcontroller, which are marked with an asterisk (Figure 8), represent a scaled version of the corresponding signals $V_{PVU}(t)$, $I_{PVU}(t)$, $V_S(t)$, V_{dsmax}, and V_{td}. Such scaling is necessary to adapt the electrical characteristics of the above signals to the limited range [0, 5] V of the microcontroller. The scaled input signals, obtained as a result of the conditioning process, are defined as follows:

$$V^*_{PVU}(t) = 5 \cdot \frac{V_{PVU}(t)}{V_{MAX}} \in [0,5]\ V \tag{16}$$

$$I^*_{PVU}(t) = 5 \cdot \frac{I_{PVU}(t)}{I_{MAX}} \in [0,5]\ V \tag{17}$$

$$V^*_S(t) = 5 \cdot \frac{V_S(t)}{V_{SSTC}} \in [0,5]\ V \tag{18}$$

$$V^*_{dsmax} = 5 \cdot \frac{V_{dsmax}}{V_{MAX}} \in [0,5]\ V \tag{19}$$

$$V^*_{td} = 5 \cdot \frac{V_{td}}{V_{tdMAX}} \in [0,5] V \tag{20}$$

where $V_{MAX} = 100$ V and $I_{MAX} = 10$ A are the maximum allowed values of the output voltage and current from the power unit, respectively.

A flowchart of the routine written in Arduino code is shown in Figure 9.

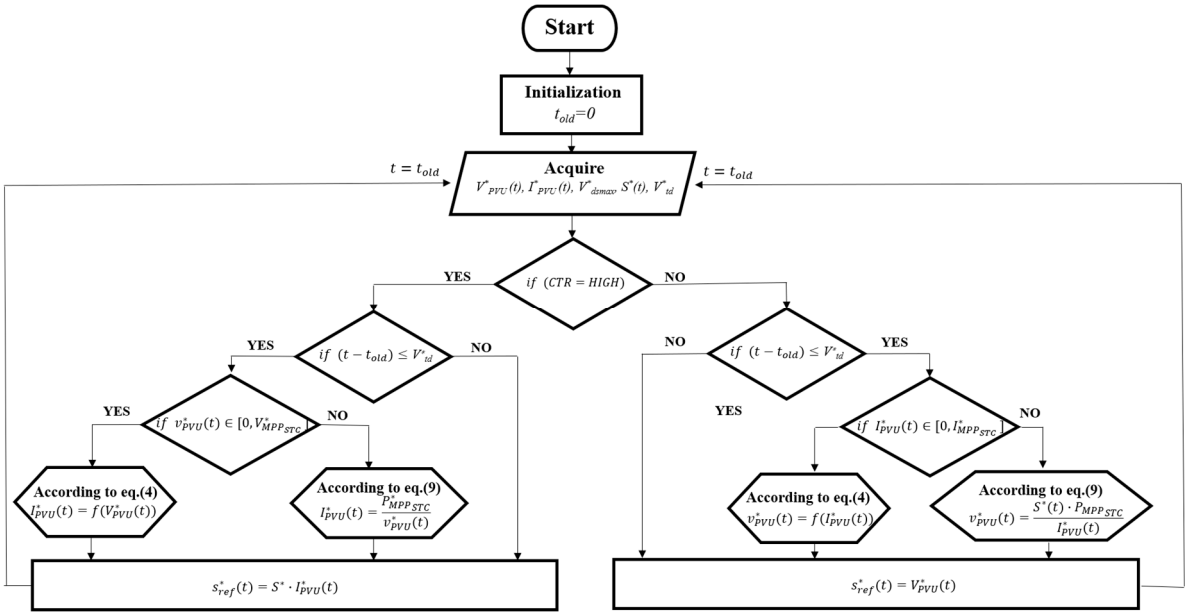

Figure 9. Flowchart of routine written in Arduino code.

In order to reduce the computation time of the code, two lookup tables (LUTs) for voltage and current controlled sources were implemented. Each LUT contains 256 samples of the scaled output variables (I^*_{PVU} and V^*_{PVU}), representing the output values I^*_{PVU} (V^*_{PVU}) calculated corresponding with the 256 value of the input signal V^*_{PVU} (I^*_{PVU}) in the range $[0, 5]$ V.

5. Experimental Results

As a first step, preliminary test activity was carried out on the sole system composed of a microcontroller board "Arduino Mega 2560" and a 12-bit, fast response Digital to Analog Converter (DAC) Adafruit (New York, USA) MCP4725, in order to check the main features of the proposed emulator. In particular, the idea was to check the capability of the emulator to reproduce the *I-V* characteristics of a Boost based photovoltaic unit for different values of irradiance $S(t)$ and maximum allowed voltage V_{dsmax} supported by the converter's mosfet. The preliminary results are shown on the display of a MDO 3034 oscilloscope by Tektronix (Beaverton, Oregon, USA), as illustrated in Figures 10 and 11. In both figures, a periodic (frequency 1 Hz) ramp signal has been applied at the microcontroller input $V^*_{PVU}(t)$ to scan the *I-V* characteristic of the proposed Boost based PVU. The amplitude of the adopted ramp signal varies from 0 to 5 V, which corresponds to PVU ramp voltage $V_{PVU}(t)$ from 0 to V_{dsmax} ($V_{dsmax} = 100$ V). The different time domain behavior of $S_{ref}(t)$ (corresponding to the output signal of the DAC) reported in Figures 11 and 12 is linked to the adoption of two different values of $V^*_S(t)$. In particular, in Figures 11 and 12, the value of $V^*_S(t)$ is equal to 2 and 1 V, corresponding to $S(t)$ equal to 400 and 200 W/m^2, respectively. By repeating the same tests with different values of $V_{dsmax} = 50$ V, the characteristics shown in Figure 12 were obtained. In this test case, the reference ramp signal rose linearly from 0 to 2.5 V.

In the next phase, the whole system was assembled and a set of representative experiments was carried out. The experimental setup was realized in the Circuit Laboratory of the University of Naples Federico II and is shown in Figure 13. It is composed of three fundamental blocks: power, control, and acquisition blocks.

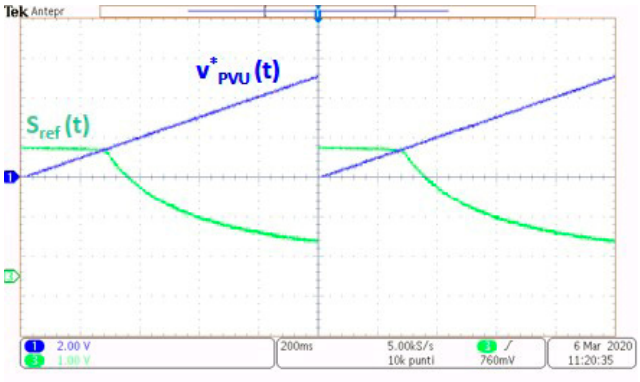

Figure 10. Oscilloscope screenshot ($S = 400$ W/m^2, $T = 57.5$ °C, and $V_{dsmax} = 100$ V).

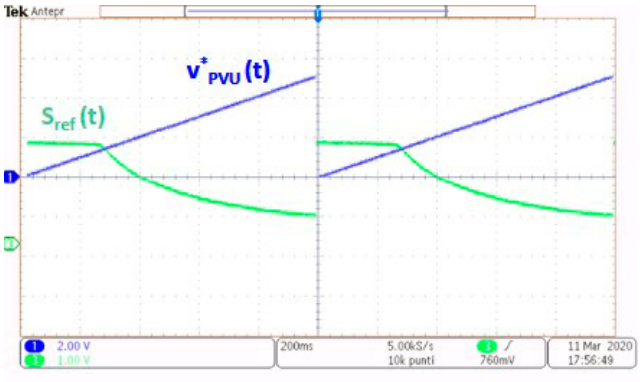

Figure 11. Oscilloscope screenshot ($S = 200$ W/m^2, $T = 57.5$ °C, and $V_{dsmax} = 100$ V).

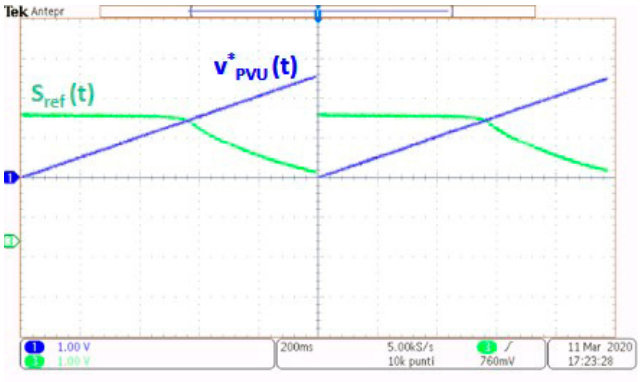

Figure 12. Oscilloscope screenshot ($S = 400$ W/m^2, $T = 57.5$ °C, and $V_{dsmax} = 50$ V).

Power block: The power block consists of two commercial power supplies BOP 100-4 [46], provided by Kepco (Flushing, New York, USA). One represents the power stage of the Boost based PV emulator and is used as a current- or voltage-controlled source. The other one is used as a controlled load in order to scan the *I-V* characteristics of the emulator. The two power supplies can work in all four quadrants of the current–voltage plane. They are linear power supplies with two bipolar control channels (voltage or current mode), selectable and individually controllable by either front panel controls or remote signals. In Table 2, the electrical characteristics of the proposed Boost based PVU emulator are reported.

Table 2. Electrical characteristics of the proposed Boost based PVU emulator.

Maximum output Current	$I_{PVUmax} = 4$ A
Maximum output Power	$P_{PVUmax} = 400$ W
Maximum output Voltage	$V_{PVUmax} = 100$ V

Control block: The core of the control block is composed of the embedded board "Arduino Mega 2560" in which the ATMega2560 microcontroller is integrated. The "Arduino Mega 2560" is powered via a USB connection and provides 54 digital input/output pins (15 of which can be used as PWM outputs) and 16 analog inputs, and it can be programmed through Arduino IDE software. Apart from the controller, the control block is composed of three units: (a) the input conditioning unit, which consists of two sensors: one current and one voltage sensor. The above sensors are used for sensing and adapting the PVU output current and voltage to the Arduino maximum allowed input voltage; (b) the output conditioning unit, which consists of the DAC MCP 4725 by Adafruit, and (c) the generation unit, which consists of the National Instruments (Austin, Texas, USA) generation board (BNC-2100 Series Connector Blocks), used to reproduce the input signals $V_S^*(t)$, V_{dsmax}^* and V_{td}^*. In order to configure the data generation hardware (BNC-2100 Series Connector Blocks) Mathworks MATLAB Data Acquisition Toolbox is used. The adopted current sensor is an INA169 module, by Texas Instruments (Dallas, Texas, USA), which allows measurement of continuous current up to 5 A. The INA169 is a "high-side, unipolar, current shunt monitor," meaning that it measures the voltage drop across a shunt resistor, which is placed on the positive power side [47]. In order to reduce the PVU output voltage up to 20 times compared to the original, a voltage divider using a resistance of 220 and 11.5 kΩ was adopted as a voltage sensor. In other words, the adopted voltage sensor is based on the series connection of two resistors. Acquisition block: During the acquisition process, the experimental data were stored and plotted in MATLAB through a commercial multichannel USB data acquisition system NI CompactDAQ, provided by National Instruments, with NI9215 modules characterized by 16-bit resolution and maximum sampling frequency of 100 kS/s).

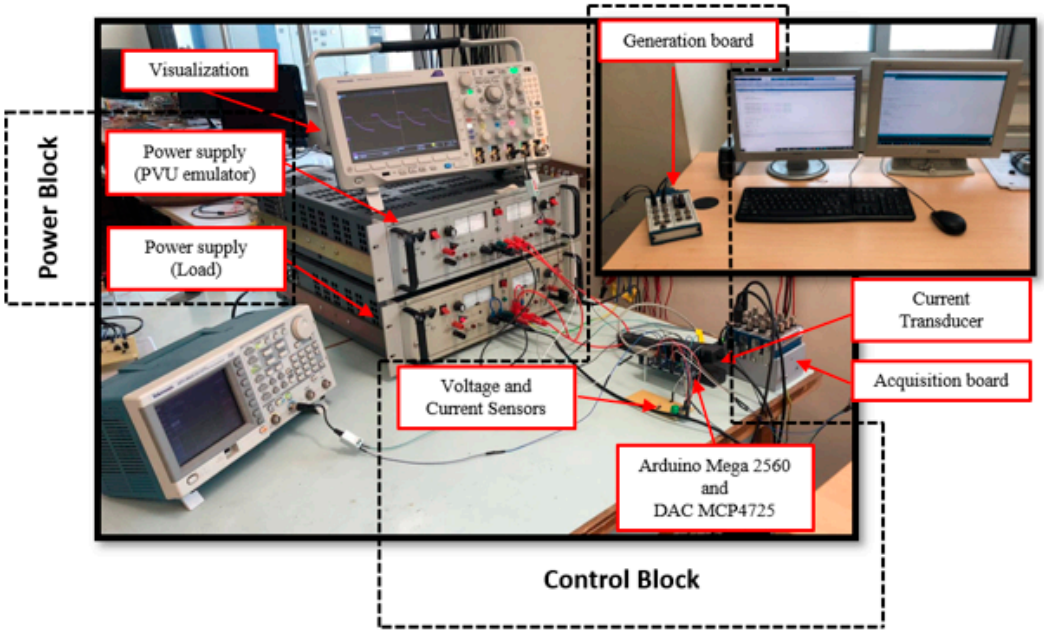

Figure 13. Experimental setup of proposed Boost based PVU emulator.

Figure 14a,b show a comparison between emulated *I-V* curves (shown in white) and theoretical curves (shown in black) in two cases. The two cases differ in the values assumed by $S(t)$ and V_{dsmax}. From these figures, it can be observed that the emulated and theoretical curves are nearly superimposed, thus confirming the excellent capability of the proposed solution of emulating PVU behavior.

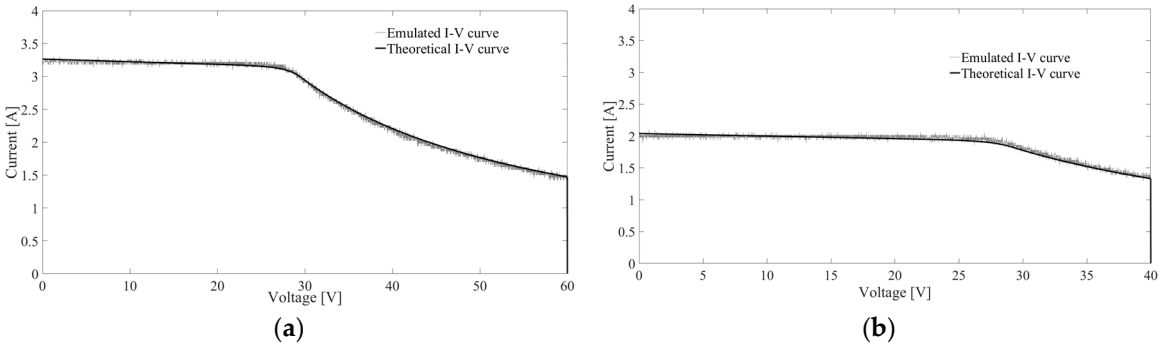

Figure 14. Comparison between emulated (grey curve) and theoretical (black curve) *I-V* curves: (**a**) $S = 400$ W/m², $T = 57.5$ °Cand $V_{dsmax} = 60$ V; (**b**) $S = 250$ W/m², $T = 57.5$ °C, and $V_{dsmax} = 40$ V.

In order to fully exploit the potential of the proposed architecture, two Boost based PVU emulators were connected in parallel (series). The performance of this system is shown in Figures 15 and 16, in which the emulated *I-V* characteristics are shown together with the corresponding theoretical ones. The effectiveness of the obtained results highlights that the proposed emulator represents a useful tool to test the performance of shaded DMPPT PV systems.

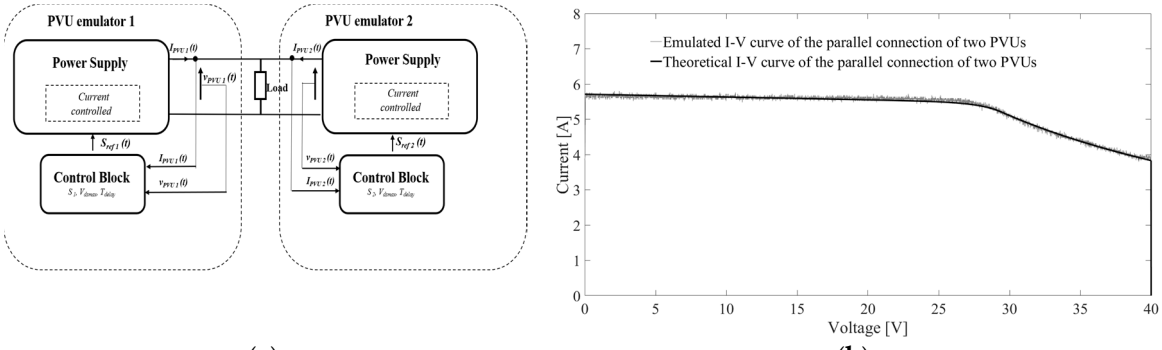

Figure 15. Performance of parallel connection of two Boost PVU emulators: (**a**) block diagram of system under test; (**b**) $S_1 = 400$ W/m², $S_2 = 300$ W/m², $T = 57.5$ °C, and $V_{dsmax} = 40$ V.

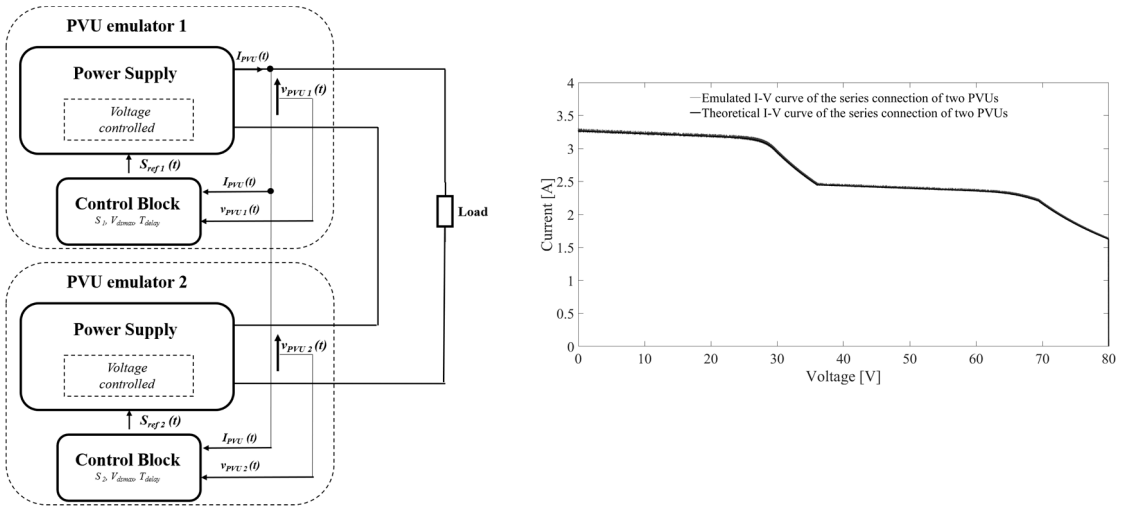

(**a**) (**b**)

Figure 16. Performance of series connection of two Boost PVU emulators: (**a**) block diagram of system under test; (**b**) $S_1 = 400$ W/m², $S_2 = 300$ W/m², $T = 57.5$ °C, and $V_{dsmax} = 40$ V.

6. Conclusions

In this paper, a Boost based PVU emulator was presented and discussed. A detailed study was carried out in order to clearly understand the mathematical model of the Boost based PVU.

The proposed emulator was designed to reproduce both $I_{PVU} = f(V_{PVU})$ and $V_{PVU} = g(I_{PVU})$ characteristics at different values not only of the irradiance levels but also of the value of V_{dsmax}. The above properties make the proposed solution suitable for fully exploring the performance of the DMPPT approach, especially when the reconfiguration technique is also applied. Moreover, the possibility to swap the value of V_{dsmax} allows emulation of a large number of Boost converters, which results in a consistent reduction in time and cost. In particular, the proposed device represents a suitable compromise between time and cost insofar as the inexpensive choice to adopt a commercial power supply is compensated by the possibility to emulate the behavior of many commercial devices. In conclusion, the main advantages of the proposed solution are the following ones; it is possible to emulate:

- both static and dynamic irradiance conditions;
- not only uniform but also mismatching operating conditions;
- both static and dynamic DMPPT configuration architectures;
- Boost based DMPPT converters with different values of V_{dsmax}.

The proposed experimental tests fully confirm the validity of the proposed emulator.

Author Contributions: Conceptualization, M.B., A.L. and C.P.; methodology, M.B.; software, M.B.; validation, M.B. A.L. and C.P.; formal analysis, M.B., A.L. and C.P.; investigation, M.B.; resources, M.B.; data curation, M.B., A.L. C.P.; writing—original draft preparation, M.B.; writing—review and editing, M.B., A.L. and C.P.; visualization, M.B. and C.P. All authors have read and agreed to the published version of the manuscript.

Funding: This research received no external funding.

Conflicts of Interest: The authors declare no conflict of interest.

Appendix A

Calculation of t_{dMAX}

In order to determine the maximum settling time t_{dMAX}, we can consider an open-loop Boost based PVU (worst case) characterized by the electrical parameters reported in Table A1 [44].

Table A1. Boost converter parameters.

Power inductor	$L = 100$ µH
Power input capacitor	$C_{in} = 220$ µF
Power output capacitor	$C_{out} = 230$ µF
Switching frequency	$f_s = 100$ kHz

In these conditions, t_{dMAX} is defined as the settling time of the step response of a well-defined transfer function (G_{vd}) of the PVU under consideration. G_{vd} is the small signal transfer function between the duty cycle and PV voltage. The expression of such a transfer function can be easily found by analyzing the small signal low-frequency equivalent circuit of a Boost based PVU and the load (Figure A1).

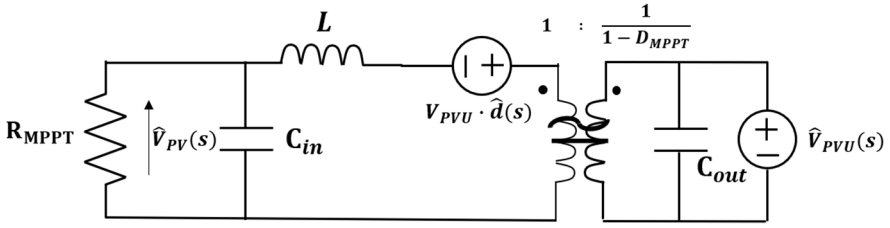

Figure A1. Small signal low-frequency equivalent circuit of Boost based PVU.

Hat symbols indicate small signal low-frequency variations [44] of the corresponding variables. The resistance R_{MPP} in Figure A1 is the differential resistance of the considered PV module [44]:

$$\boldsymbol{R_{MPP} = \frac{V_{MPP_{STC}}}{I_{MPP_{STC}}}} \quad \text{(A1)}$$

The expression of G_{vd} is:

$$\boldsymbol{G_{vd}(s) = \frac{\hat{V}_{PV}(s)}{\hat{d}(s)} = -V_{PVU} \cdot \left(\frac{1}{1 + \frac{sL}{R_{MPP}} + S^2 L C_{in}} \right)} \quad \text{(A2)}$$

The settling time (t_{dMAX}) of the step response of the above transfer function is equal to about 10 ms, if:

$$\boldsymbol{V_{PVU} = V_{MAX} = 100\ V} \quad \text{(A3)}$$

$$\boldsymbol{D_{MPPT} = \left(1 - \frac{V_{MPP_{STC}}}{V_{MAX}}\right) \cong 0.7} \quad \text{(A4)}$$

References

1. Kaushika, N.D.; Rai, A.K. An investigation of mismatch losses in solar photovoltaic cell networks. *Energy* **2007**, *325*, 755–759.
2. Baltus, C.W.A.; Eikelboom, J.A.; Van Zolingen, R.J.C. Analytical Monitoring of Losses in PV Systems. In Proceedings of the 14th European Photovoltaic Solar Energy Conference, Barcelona, Spain, 30 June–4 July 1997; pp. 1547–1550.
3. Bucciarelli, L.L., Jr. Power loss in photovoltaic arrays due to mismatch in cell characteristics. *Sol. Energy* **1979**, *23*, 277–288.

4. King, D.L.; Boyson, W.E.; Kratochvil, J.A. Analysis of Factors Influencing the Annual Energy Production of Photovoltaic Systems. In Proceedings of the 29th IEEE Photovoltaic Specialists Conference, New Orleans, LA, USA, 19–24 May 2002; pp. 1356–1361.
5. Zilles, R.; Lorenzo, E. An Analytical Model for Mismatch Losses in PV Arrays. *Int. J. Sol. Energy* **1992**, *13*, 121–133.
6. Chamberlin, C.E.; Lehman, P.; Zoellick, J.; Pauletto, G. Effects of Mismatch Losses in Photovoltaic Arrays. *Sol. Energy* **1995**, *543*, 165–171.
7. Manganiello, P.; Balato, M.; Vitelli, M. A Survey on Mismatching and Aging of PV Modules: The Closed Loop. *IEEE Trans. Ind. Electron.* **2015**, *62*, 7276–7286. doi:10.1109/TIE.2015.2418731.
8. Sera, D.; Mathe, L.; Kerekes, T.; Spataru, S.V.; Teodorescu, R. On the perturb-and-observe and incremental conductance MPPT methods for PV systems. *IEEE J. Photovolt.* **2013**, *3*, 1070–1078.
9. Chiu, C.-S. T-S fuzzy maximum power point tracking control of solar power generation systems. *IEEE Trans. Energy Convers.* **2010**, *25*, 1123–1132.
10. Macaulay, J.; Zhou, Z. A Fuzzy Logical-Based Variable Step Size P&O MPPT Algorithm for Photovoltaic System. *Energies* **2018**, *11*, 1340.
11. Kolesnik, S.; Kuperman, A. On the equivalence of major variable-step-size MPPT algorithms. *IEEE J. Photovolt.* **2016**, *6*, 590–594. doi:10.1109/JPHOTOV.2016.2520212.
12. Sokolov, M.; Shmilovitz, D. A modified MPPT scheme for accelerated convergence. *IEEE Trans. Energy Convers.* **2008**, *23*, 1105–1107. doi:10.1109/TEC.2008.2001464.
13. Balato, M.; Costanzo, L.; Vitelli, M. Maximum power point tracking techniques. In *Wiley Online Encyclopedia of Electrical and Electronics Engineering*; John Wiley & Sons: Somerset, NJ, USA, 2016; pp. 1–26. doi:10.1002/0477134608X.W8299.
14. Kumar, G.; Trivedi, M.B.; Panchal, A.K. Innovative and precise MPP estimation using P–V curve geometry for photovoltaics. *Appl. Energy* **2015**, *138*, 640–647.
15. Kumar, G.; Panchal, A.K. Geometrical prediction of maximum power point for photovoltaics. *Appl. Energy* **2014**, *119*, 237–245.
16. Femia, N.; Petrone, G.; Spagnuolo, G.; Vitelli, M. Optimization of perturb and observe maximum power point tracking method. *IEEE Trans. Power Electron.* **2015**, *20*, 963–973.
17. Nguyen, D.; Lehman, B. An adaptive solar photovoltaic array using model-based reconfiguration algorithm. *IEEE Trans. Ind. Electron.* **2008**, *55*, 2644–2654.
18. Villa, L.F.L.; Picault, D.; Raison, B.; Bacha, S.; Labonne, A. Maximizing the power output of partially shaded photovoltaic plants through optimization of the interconnections among its modules. *IEEE J. Photovolt.* **2012**, *2*, 154–163.
19. Obane, H.; Okajima, K.; Oozeki, T.; Ishii, T. PV system with reconnection to improve output under nonuniform illumination. *IEEE J. Photovolt.* **2012**, *2*, 341–347.
20. Obane, H.; Okajima, K.; Oozeki, T.; Ishii, T. PV System with Reconnection to Improve Output Under Nonuniform Illumination. *IEEE J. Photovol.* **2012**, *2*, 341–347.
21. Storey, J.; Wilson, P.; Bagnall, D. Improved optimization strategy for irradiance equalization in dynamic photovoltaic arrays. *IEEE Trans. Power Electron.* **2013**, *28*, 2946–2956.
22. Sanseverino, E.R.; Ngoc, T.N.; Cardinale, M.; Vigni, V.L.; Musso, D.; Romano, P.; Viola, F. Dynamic programming and Munkres algorithm for optimal photovoltaic arrays reconfiguration. *Sol. Energy* **2015**, *122*, 347–358.
23. La Manna, D.; Vigni, V.L.; Sanseverino, E.R.; Di Dio, V.; Romano, P. Reconfigurable electrical interconnection strategies for photovoltaic arrays: A review. *Renew. Sustain. Energy Rev.* **2014**, *33*, 412–426.
24. Balato, M.; Costanzo, L.; Vitelli, M. Reconfiguration of PV modules: A tool to get the best compromise between maximization of the extracted power and minimization of localized heating phenomena. *Sol. Energy* **2016**, *138*, 105–118.
25. Balato, M.; Costanzo, L.; Vitelli, M. Series–Parallel PV array re-configuration: Maximization of the extraction of energy and much more. *Appl. Energy* **2015**, *159*, 145–160.
26. Balato, M.; Costanzo, L.; Vitelli, M. Multi-objective optimization of PV arrays performances by means of the dynamical reconfiguration of PV modules connections. In Proceedings of the International Conference on Renewable Energy Research and Applications ICRERA 2015, Palermo, Italy, 22–25 November 2015; pp. 1646–1650.

27. Burger, B.; Goeldi, B.; Rogalla, S.; Schmidt, H. Module integrated electronics e an overview. In Proceedings of the 25th European Photovoltaic Solar Energy Conference and Exhibition, Valencia, Spain, 6–10 September 2010; pp. 3700–3707.
28. Li, Q.; Wolfs, P. A review of the single-phase photovoltaic module integrated converter topologies with three different DC link configurations. *IEEE Trans. Power Electron.* **2008**, *23*, 1320–1333.
29. Kjaer, S.B.; Pedersen, J.K.; Blaabjerg, F. A review of single-phase grid-connected inverters for photovoltaic modules. *IEEE Trans. Ind. Appl.* **2005**, *41*, 1292–1306.
30. Femia, N.; Lisi, G.; Petrone, G.; Spagnuolo, G.; Vitelli, M. Distributed maximum power point tracking of photovoltaic arrays: Novel approach and system analysis. *IEEE Trans. Ind. Electron.* **2008**, *55*, 2610–2621.
31. Walker, G.R.; Sernia, P.C. Cascaded DC-DC converter connection of photovoltaic modules. *IEEE Trans. Power Electron.* **2004**, *19*, 1130–1139.
32. Roman, E.; Alonso, R.; Ibanez, P.; Elorduizapatarietxe, S.; Goitia, D. Intelligent PV module for grid-connected PV systems. *IEEE Trans. Ind. Electron.* **2006**, *53*, 1066–1073.
33. Balato, M.; Costanzo, L.; Marino, P.; Rubino, G.; Rubino, L.; Vitelli, M. Modified TEODI MPPT technique: Theoretical analysis and experimental validation in uniform and mismatching conditions. *IEEE J. Photovolt.* **2017**, *2*, 604–613.
34. Ramos-Paja, C.A.; Gira, R.; Arango-Zuluaga, E.I. Distributed maximum power point tracking in photovoltaic applications: Active bypass DC/DC converter. *Rev. Fac. Ing. Univ. Antioq.* **2012**, *64*, 32–44.
35. Balato, M.; Vitelli, M. A new control strategy for the optimization of Distributed MPPT in PV applications. *Int. J. Electr. Power Energy Syst.* **2014**, *62*, 763–773.
36. Balato, M.; Vitelli, M.; Femia, N.; Petrone, G.; Spagnuolo, G. Factors limiting the efficiency of DMPPT in PV applications. In Proceedings of the 2011 International Conference on Clean Electrical Power (ICCEP), Ischia, Italy, 14–16 June 2011; pp. 604–608. doi:10.1109/ICCEP.2011.6036319.
37. Balato, M.; Costanzo, L.; Vitelli, M. DMPPT PV system: Modeling and control techniques. *Adv. Renew. Energ. Power. Technol.* **2018**, *1*, 163–205.
38. Balato, M.; Petrarca, C. The Impact of Reconfiguration on the Energy Performance of the Distributed Maximum Power Point Tracking Approach in PV Plants. *Energies* **2020**, *13*, 1511.
39. Balato, M.; Costanzo, L.; Gallo, D.; Landi, C.; Luiso, M.; Vitelli, M. Design and implementation of a dynamic FPAA based photovoltaic emulator. *Sol. Energy* **2016**, *123*, 102–115. doi:10.1016/j.solener.2015.11.006.
40. Chalh, A.; Motahhir, S.; El Hammoumi, A.; El Ghzizal, A.; Derouich, A. Study of a Low-Cost PV Emulator for Testing MPPT Algorithm Under Fast Irradiation and Temperature Change. *Technol. Econ. Smart Grids Sustain. Energy* **2018**, *3*, 11. doi:10.1007/s40866-018-0047-8.
41. Moussa, I.; Khedher, A.; Bouallegue, A. Design of a Low-Cost PV Emulator Applied for PVECS. *Electronics* **2019**, *8*, 232.
42. Ullah, N.; Nisar, F.; Alahmadi, A.A. Closed Loop Control of Photo Voltaic Emulator Using Fractional Calculus. *IEEE Access* **2020**, *8*, 28880–28887.
43. Sunmodule Solar Panel 225 Mono Ds. Available online: www.solarworld-usa.com/~/media/www/files/datasheets/sunmodule-plus/sunmodule-solar-panel-225-mono-ds.pdf.(accessed on June 3rd 2020)
44. Femia, N.; Petrone, G.; Spagnuolo, G.; Vitelli, M. *Power Electronics and Control Techniques for Maximum Energy Harvesting in Photovoltaic Systems*; CRC Press, Taylor & Francis group: Boca Raton, FL, USA, 2012.
45. Arduino Web Editor. Available online: https://www.arduino.cc/en/main/software.(accessed on June 3rd 2020)
46. Series BOP: Linear Power Supplies, Bipolar 4-quadrant, Analog/Digital/Local Control, Ultra Low Ripple/Noise. Available online: https://www.kepcopower.com/bop.htm.(accessed on June 3rd 2020)
47. INA1x9 High-Side Measurement Current Shunt Monitor. Available online: http://www.ti.com/lit/ds/symlink/ina169.pdf?ts=1590582981664.(accessed on June 3rd 2020)